Science of Sintering, **55** (2023) 259-268

https://doi.org/10.2298/SOS220916010E

UDK: 676.017.2; 53.086

Influence of Raster Angle on Tensile Properties of FDM Additively Manufactured Plates made from Carbon Reinforced PET-G Material

Abdelnaser A. Elayeb[1], Milan Janković[1*)], Stefan Dikić[2], Dragoljub Bekrić[1], Igor Balać[1]

[1]University of Belgrade, Faculty of Mechanical Engineering, Kraljice Marije 16, 11000 Belgrade, Serbia

[2]University of Belgrade, Faculty of Technology and Metallurgy, Karnegijeva 4, 11000 Belgrade, Serbia

Abstract:

Tensile properties of thin plate specimens made from short carbon fiber reinforced PET-G material are experimentally evaluated for various raster angles (printing directions). In additive manufacturing (AM), raster angle is recognized as one of the key printing parameters which strongly influences the strength and stiffness of the final part. The relatively high average value of ultimate tensile strength was obtained for specimens printed with the 0° raster angle, compared to the value obtained for specimens printed with the 90° raster angle - 52.2 MPa and 25.4 MPa, respectively. Similarly, noticeably higher average value of modulus of elasticity was obtained for specimens printed with the 0° raster angle, compared to the value obtained for specimens printed with the 90° raster angle - 4752 MPa and 1569 MPa, respectively. Scanning electron microscopy (SEM) was used for analysis of specimens' fracture surfaces. SEM images revealed considerable volume fraction of voids (porosity). The porosity, together with weak bonding between two adjacent rasters, could be one of key factors for poor tensile properties of samples printed with rasters perpendicular to direction of load application (90° raster angle).

Keywords*: Additive manufacturing raster angle; Strength; Stiffness; Carbon fibers.*

1. Introduction

The use of polymers in fabricating functional parts by additive manufacturing (AM) methods has been gaining attention of the industry for past two decades due to possibility of fabricating complex three-dimensional components while putting in less effort and time compared to conventional machining processes, as well as its convenient operation, low cost, versatile feedstock materials, great design flexibility and waste-free production [1-3]. Extrusion based AM, known as fused deposition modelling (FDM) or fused filament fabrication (FFF), has become a widespread AM technique. As a result, the development and production of polymer-based parts via AM is a continuously emerging research trend [4]. Common feedstock materials for FDM process are polymers such as: acrylonitrile butadiene styrene (ABS), polylactic acid (PLA) and polycarbonate (PC) [5]. Tensile strength of samples made from these materials is found to be in the range of 20-60 MPa [6]. For most polymers commonly used in AM stiffness values roughly range from 1 to 2 GPa [7]. Although

*) **Corresponding author:** mmjankovic@mas.bg.ac.rs

polymers have much lower strength and stiffness than metals, they have significantly lower density and in some cases polymers may have higher strength per unit weight than metals.

Since polymers have limited mechanical properties, aiming to make FDM suitable for producing functional load-bearing parts, short carbon fibers have been introduced into polymeric feedstock materials as reinforcements [8]. Besides short fibers, continuous fibers and particulates can also be added as reinforcements of polymers used to fabricate parts through FDM. Compared to printed parts made from neat polymer, components made of reinforced polymer have enhanced mechanical properties [8-15]. Although continuous fiber reinforced composites offer high mechanical performance, their processing through FDM is not commonplace due to printing complexity [16]. On the other hand, short fiber reinforced polymers (SFRPs) are used more often due to availability of feedstock materials and low-cost fabrication, but with moderately improved mechanical properties [17-19].

In extrusion-based AM final printed part has material properties which differ from those of the filament material used for its fabrication. This difference mainly arises from: build orientation (*flat, on-edge, upright* – see Fig. 1), printing direction, layer thickness, infill density, overlapping, infill print speed, nozzle temperature and printing bed temperature [20-22]. In addition, presence of porosity within the material should also be considered since it degrades mechanical properties such as strength and stiffness, which is particularly important when material is used for producing structural members intended for carrying load [23,24]. Despite the fact that AM offers considerable freedom in design and production of 3D printed parts, anisotropy and inhomogeneity remain primary concerns [25,26].

Alongside the fact that the aforementioned parameters of printing process affect final mechanical properties, raster angle (printing direction) appear to be one of the main influential parameters, especially for parts printed with flat orientation [3,25]. Raster angle θ is the angle between the direction of the deposited beads and the *x*-axis (axis of load application), as shown in Fig. 2. Therefore, major objective of this paper is to determine the tensile properties of FDM additively manufactured thin plate specimens made from carbon reinforced polyethylene terephthalate with added glycol (PET-G) material for different raster angles.

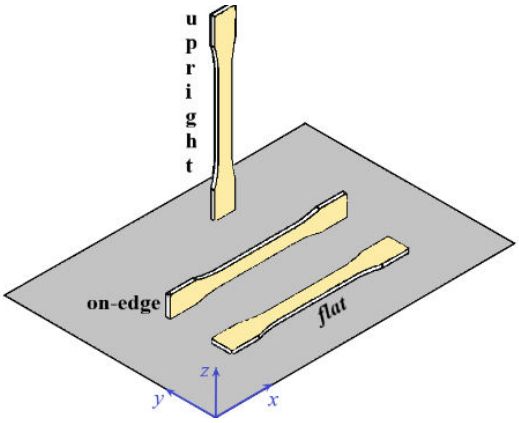

Fig. 1. Build orientation in FDM.

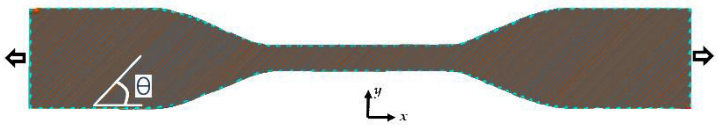

Fig. 2. Schematic of raster angle (θ) in a 3D printed part.

2. Materials and Experimental Procedures

Tensile properties of test specimens fabricated using PET-G material reinforced with carbon fiber fragments are examined. Flat build orientation was employed for fabrication. The ultimate tensile strength and stiffness are evaluated experimentally for specimens made with different raster angles, ranging from 0° to 90° with an increment of 15°.

Test specimens are printed as per ASTM D638-03 – the Type I. Series of five test specimens of each considered raster angle (0°, 15°, 30°, 45°, 60°, 75°, 90°, respectively) were printed – Fig. 3. Black Element's PET-G filament with 30% weight fraction of short carbon fibers as reinforcements is used for printing the specimens. Since carbon fiber reinforced filaments are extremely abrasive, steel nozzle was used to ensure wear resistance. Diameter of the nozzle was 0.4 mm. Printing parameters such as hot end temperature 250°C, heated bed temperature 90°C, speed 80mm/s, extrusion width 0.45 mm, layer thickness 0.2mm and infill density 100% with 25% overlapping were employed while fabricating the test specimens using Prusa MINI+ 3D printer. The infill density and overlapping were set to 100% and 25% respectively aiming to minimise the air gap. Usually, an air gap (captured air) appears between two adjacent rasters or beads. Although overlapping may result in uneven surfaces, dimensional inequality and extended printing times, it can considerably improve the integrity of the part, minimize air gap and also facilitate diffusions between adjacent layers [27,28]. All the specimens were printed without contour lines to prevent them from affecting output mechanical properties.

Fig. 3. Series of printed samples prepared for testing.

Fig. 4. Experimental setup used for the tensile test.

Series of samples were tested to the breaking point on the Shimadzu AG-Xplus tensile testing machine (Fig. 4), while ongoing results (force and current elongation) were being recorded through built-in software – Trapezium X. Speed of testing was set to 2.5 mm/min. During the actual test on the universal testing machine, extensional strain rates of samples were recorded using Digital Image Correlation (DIC). Scanning electron microscopy (SEM) was used for analysing the fracture surfaces of tested specimens.

3. Results and Discussion

Based on data from universal testing machine the stress-strain diagrams were formed – Fig. 5, wherefrom the mean values of modulus of elasticity and ultimate tensile stress were determined for each of the seven observed cases. It is obvious that all of the tested samples have region of linear-elastic behaviour on stress-strain curve. The transition between elastic and inelastic region on the stress-strain curve is not clear for the tested material. All samples broke shortly afterwards reaching the ultimate strength. Values for ultimate tensile strengths are directly calculated from recorded data as maximum stresses withstood throughout the testing.

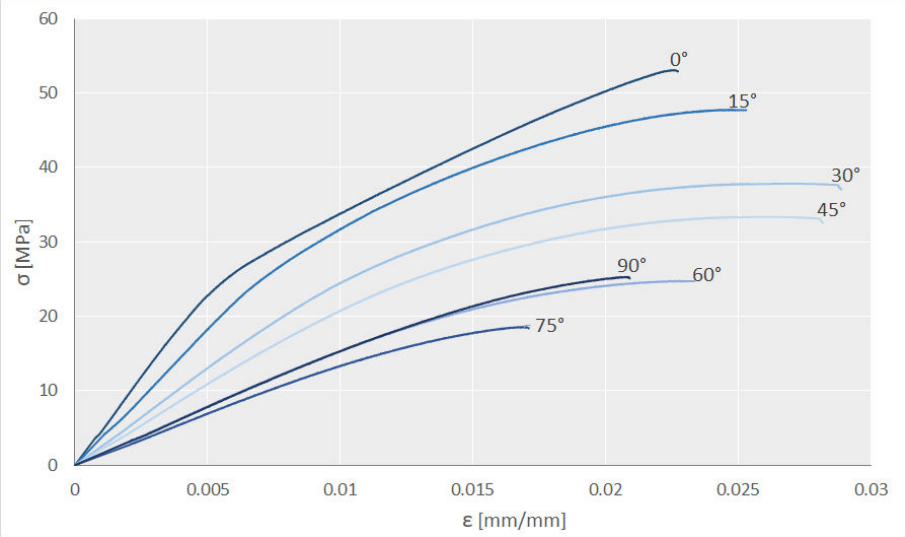

Fig. 5. Stress-strain curves for different raster angles.

In order to obtain correct values of the recorded strain, toe compensation is performed on the original stress-strain curves derived from universal testing machine data to get the corrected zero point of strain axis resulting in curves shown in Fig. 5. Then, constructing tangents to linear-elastic parts of the stress-strain curves enabled evaluating corresponding slopes representing moduli of elasticity (see Fig. 6). The average and standard deviation values for modulus of elasticity and ultimate tensile strength are listed in Table I. The standard deviation of all measurements is small, and this indicates good repeatability in the experimental data.

Bar graph in Fig. 7a emphasizes difference in calculated values of the modulus of elasticity for different raster angles. It is obvious that specimens printed with the 0° raster angle possess considerably higher stiffness than those printed utilizing the 60°, 75° and 90° raster angles. Therefore, it is evident that mechanical anisotropy occurs due to change in raster angle. The average values of the ultimate tensile strength are outlined in Fig. 7b. Samples printed with the 0° raster angle proved to have the highest strength values, while

those printed with the 75° raster angle showed the lowest ones. Although a minimum value of the ultimate tensile strength was expected for samples printed with the 90° raster angle, the minimum value obtained for samples printed with the 75° raster angle can be explained by the anisotropic property of the tested material.

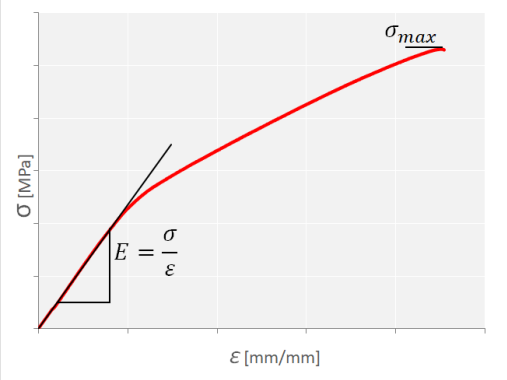

Fig. 6. Graphical method for calculating modulus of elasticity (slope of the curve).

Tab. I Summary of values for modulus of elasticity and ultimate tensile strength acquired for different raster angles.

Raster angle [°]	E [MPa]		σ_{max} [MPa]	
	Average	St.Dev.	Average	St.Dev.
0	4752	106	52.2	2.5
15	3709	112	47.8	0.8
30	2664	64	37.8	0.4
45	2089	61	33.1	0.5
60	1573	15	24.7	0.9
75	1393	33	19.0	0.6
90	1569	26	25.4	0.4

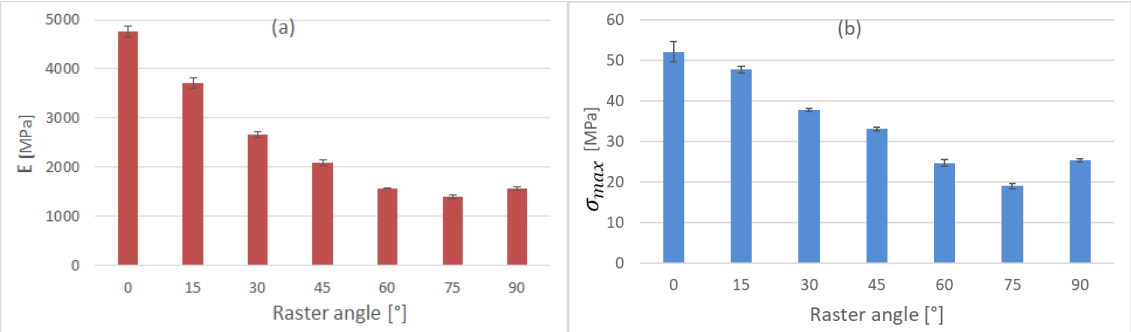

Fig. 7. Variation of modulus of elasticity (a) and ultimate tensile strength (b) with change in raster angle.

Fracture surfaces of the tested specimens with the 0° and 90° raster angles were recorded using SEM, as shown in Figs. 8. and 9. Recorded SEM images enabled inspecting the inhomogeneity of the tested specimen in region of fracture zone as well as orientation of the introduced carbon fibers relative to the applied printing direction.

Fracture surface of the specimen printed with the 0° raster angle is presented in Fig. 8a showing cross section of one raster and air gap formed around it. Some of detected carbon

fibers are circled in yellow. Raster width of 425 µm, as highlighted in Fig. 8a, corresponds to the preassigned extrusion width. It is noticeable that the fibers are mostly aligned with the direction of printing. In this case they are pointing out of the image (direction normal to image plane). Carbon fibers and their orientation are more clearly visible in the Fig. 8b. Therefore, it is proved that fibers generally align within the flow of printing direction and this could be the main reason why specimens fabricated with the 0° raster angle showed the highest value of ultimate strength.

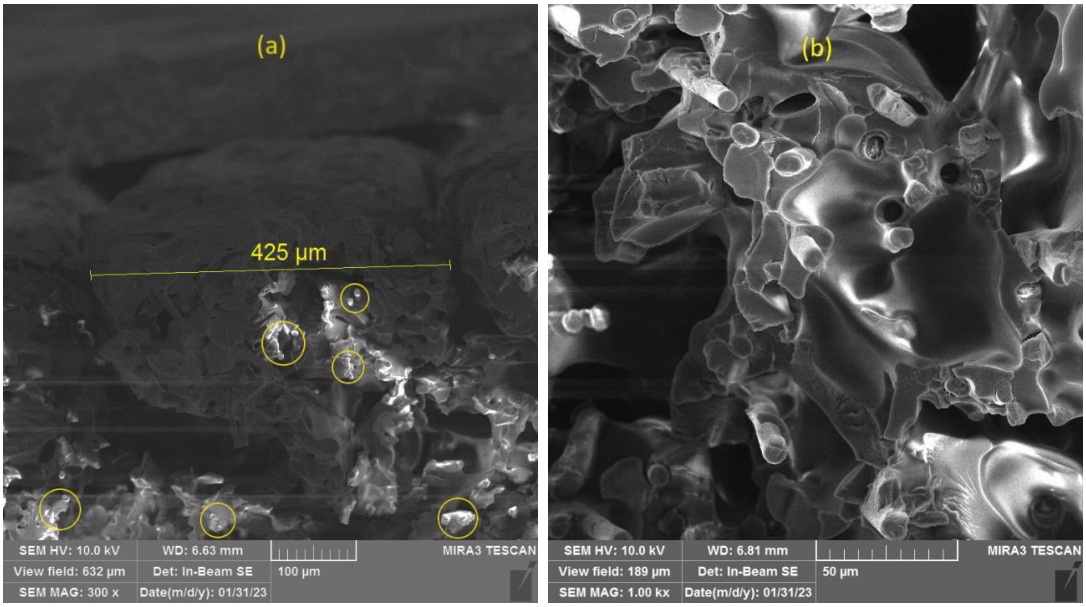

Fig. 8. SEM images of fracture surface of the specimen printed with 0° raster angle: (a) raster cross-section together with air gap around it – 300 x magnification; (b) orientation of carbon fibers – 1000 x magnification.

The 90° raster angle specimen's fracture surface is depicted in Fig. 9a with a clear border between subsequent layers. As expected, major voids are positioned between the deposited rasters (beads) in form of captured air. Measures of 213 µm and 221 µm, highlighted in Fig. 9.a, are in compliance with the preassigned printing parameter – layer thickness of 0.2 mm. Final orientation of carbon fibers in this case is more visible in Fig. 9b. Based on traces where fibers were placed before being pulled out during the fracure, it can be concluded that fibers are again generally aligned with the direction of the deposited rasters. This is also proved by the orientation of fibers that remained on the fracture surface of the observed specimen's part – fibers circled in yellow in Fig. 9b. Such carbon fibers alignment (perpendicular to direction of load application) together with presence of voids and week bonding between two adjacent rasters could be the major reason for poor tensile properties of the 90° raster angle specimens.

After analyzing the recorded SEM images, it is concluded that there is certain amount of carbon fibers which are not aligned with the printing direction. These are the fibers which probably did not bond properly with the polymer during the filament production process itself. One of such fibers is circled in red in Fig. 9b. However, it is important to emphasize that there is a small amount of such fibers compared to those which are properly "wetted" and follow the printing direction. An example of interface bonding between fiber and polymer is shown in Fig. 10a, with measured diameter of the fiber highlighted (9 µm). An example of a fiber with poor bonding is presented in Fig. 10b – closer look at the fiber previously circled in red in Fig. 9b.

Although the overlapping was set to 25% with intention to minimize the air gap, according to SEM images the raster geometry inherently formed visible spaces of captured air which are present in each layer and/or between layers as well as between adjacent rasters. Based on recorded SEM images, voids are also present within a polymer phase (porosity) as well as on interface between carbon fibers and PET-G polymer. Except the decrease of the physical cross-sectional area causing the decrease of effective elastic moduli, the presence of such voids may lead to high stress concentration factors, thus reducing the tensile strength of tested samples.

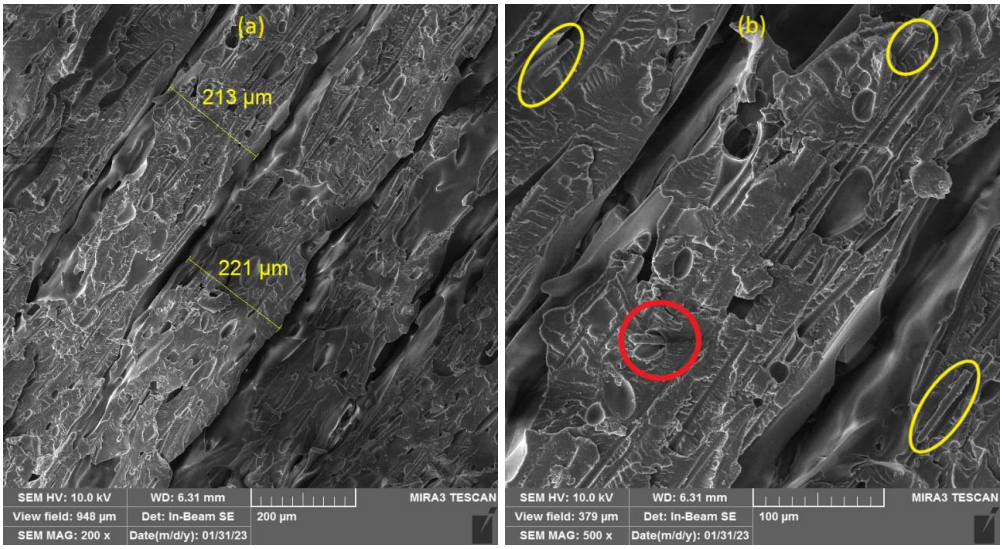

Fig. 9. SEM images of fracture surface of the specimen printed with 90° raster angle: (a) layers clearly visible with border between them in form of captured air – 200 x magnification; (b) orientation of carbon fibers – 500 x magnification.

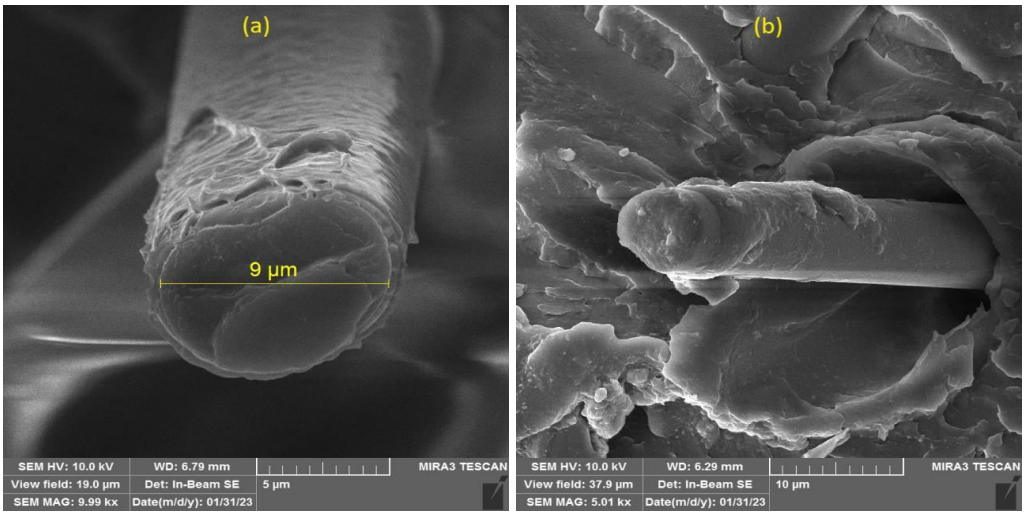

Fig. 10. SEM images of (a) an example of good interface bonding between fiber and polymer, with measured diameter of the fiber highlighted – 10000 x magnification and (b) an example of bonding – 5000 x magnification.

Despite SEM images confirmed that carbon fibers mostly align with the printing direction, significant level of voids in printed material may be the key reason for relatively

low value of ultimate tensile strength (52.2 MPa) obtained for samples printed with the 0° raster angle, when compared to the maximum value of 46.1 MPa obtained for neat PET-G [8].

4. Conclusion

The effect of raster angle on tensile properties of thin plate specimens made from carbon reinforced PET-G material was studied. It is confirmed that raster angle strongly influences the strength and stiffness of final additively manufactured thin plate parts. The relatively high average value of ultimate tensile strength - 52.2 MPa was obtained for specimens printed with the raster angle of 0°, compared to the value obtained for specimens printed with the raster angle of 90° - 25.4 MPa. The minimum average value of ultimate tensile strength was obtained for specimens printed with the raster angle of 75° - 19.0 MPa which indicates decrease of 63.6% (compared to value for the 0° raster angle). Similarly, the maximum obtained average value of modulus of elasticity - 4752 MPa was obtained for specimens printed with the raster angle of 0° compared to the value of 1569 MPa, obtained for specimens printed with the raster angle of 90°. Again, the minimum average value of modulus of elasticity was obtained for specimens printed with the raster angle of 75° - 1393 MPa, which indicates decrease of 70.7%.

SEM images of fracture surfaces of the specimens printed with the 0° raster angle revealed dominant alignment of carbon fibers with the printing direction applied, but also moderate to high level of inhomogeneity and voids. Considerable volume fraction of captured air (air gaps) with noticeable amount of porosity in polymer phase are probably major factors which resulted in relatively low improvement of tensile strength obtained for carbon reinforced samples made with the 0° printing direction, when compared to neat polymer samples. In the similar manner, voids together with weak bonding between two adjacent rasters undoubtedly contributed to poor tensile properties of carbon reinforced samples made with the raster angle of 90°.

Acknowledgments

This research has been financed by the Ministry of Science, Technological Development and Innovation of the Republic of Serbia – Grant No. 451-03-47/2023-01/ 200105.

5. References

1. M. Spoerk, C. Savandaiah, F. Arbeiter, G. Traxler, L. Cardon, C. Holzer, J. Sapkota, Anisotropic properties of oriented short carbon fibre filled polypropylene parts fabricated by extrusion-based additive manufacturing, Composites Part A 113 (2018) 95-104.
2. E. Cuan-Urquizo, E. Barocio, V. Tejada-Ortigoza, R. B. Pipes, C. A. Rodriguez, A. Roman-Flores, Characterization of the Mechanical Properties of FFF Structures and Materials: A Review on the Experimental, Computational and Theoretical Approaches, Materials, 12, 6 (2019) 895.
3. M. Somireddy, C.V. Singh, A. Czekanski, Mechanical behaviour of 3D printed composite parts with short carbon fiber reinforcements, Engineering Failure Analysis, 107 (2019) 104232.

4. Z. Quan, A. Wu, M. Keefe, X. Qin, J. Yu, J. Suhr, J-H. Byun, B-S. Kim, T-W. Chou, Additive manufacturing of multi-directional preforms for composites: Opportunities and challenges, Materials Today, 18(9) (2015) 503-512.
5. K.M. Pradeep, P. Senthil, Prediction of in-plane stiffness of multi-material 3D printed laminate parts fabricated by FDM process using CLT and its mechanical behaviour under tensile load, Materials Today Communications 23 (2020) 100955
6. A. Maguire, N. Pottackal., M.A.S.R. Saadi, M.M. Rahman, P. Ajayan, Additive manufacturing of polymer-based structures by extrusion technologies, Review article, Oxford Open Materials Science, 1(1) (2021) itaa004.
7. J.R. Dizon, A.H. Espera Jr., Q. Chen, R. C. Advincula, Mechanical characterization of 3D-printed polymers, Additive Manufacturing, 20 (2018) 44-67.
8. D. Jiang, D. E. Smith, Anisotropic mechanical properties of oriented carbon fiber filled polymer composites produced with fused filament fabrication, Additive Manufacturing 18 (2017) 84–94.
9. R. Matsuzaki, M. Ueda, M. Namiki, T.K. Jeong, H. Asahara, K. Horiguchi, T. Nakamura, A. Todoroki, Y. Hirano, Three-dimensional printing of continuous-fiber composites by in-nozzle impregnation. Sci Rep. 6 (2016) 23058
10. X. Tian, A. Todoroki, T. Liu, L. Wu, Z. Hou, M. Ueda, Y. Hirano, R. Matsuzaki, K. Mizukami, K. Iizuka, A. V. Malakhov, A. N. Polilov, D. Li, B. Lu, 3D printing of continuous fiber reinforced polymer composites: Development, Application and Prospective, Chinese Journal of Mechanical Engineering: Additive Manufacturing Frontiers 1 (2022) 100016.
11. J. Justo, L. Távara, L. García-Guzmán, F. París, Characterization of 3D printed long fibre reinforced composites, Composite Structures 185 (2018) 537-548.
12. W. Zhang, A.S. Wu, J. Sun, Z. Quan, B. Gu, B. Sun, C. Cotton, D. Heider, T-W. Chou, Characterization of residual stress and deformation in additively manufactured ABS polymer and composite specimens, Composites Science and Technology, 150 (2017) 102-110.
13. G. Liao, Z. Li, Y. Cheng, D. Xu, D. Zhu, S. Jiang, J. Guo, X. Chen, G. Xu, Y. Zhu, Properties of oriented carbon fiber/polyamide 12 composite parts fabricated by fused deposition modelling, Materials and Design 139 (2018) 283-292.
14. N.G. Karsli, A. Aytac, Tensile and thermomechanical properties of short carbon fiber reinforced polyamide 6 composites, Composites Part B 51 (2013) 270-275.
15. E.C. Botelho, L. Figiel, M.C. Rezende, B. Lauke. Mechanical behavior of carbon fiber reinforced polyamide composites, Composites Science and Technology 63 (2003) 1843-1855.
16. H. L. Tekinalp, V. Kunc, G. M. Velez-Garcia, C. E. Duty, L. J. Love, A. K. Naskar, C. A. Blue, S. Ozcan, Highly oriented carbon fiber–polymer composites via additive manufacturing, Composites Science and Technology 105 (2014) 144–150.
17. S.Y. Fu, B. Lauke, E. Mader, C.Y. Yue, X. Hu, Tensile properties of short-glass-fiber and short-carbon-fiber-reinforced polypropylene composites, Composites: Part A 31 (2000) 1117-1125.
18. R.J. Kuriger, M.K. Alam, D.P. Anderson, R.L. Jacobson, Processing and characterization of aligned vapor grown carbon fiber reinforced polypropylene, Composites Part A 33 (2002) 53-62.
19. S.Y. Fu, B. Lauke,. Effect of fiber length and fiber orientation distributions on the tensile strength of short-fiber-reinforced polymers. Composites Science and Technology, 56 (1996) 1179-1190.
20. J.M. Chacón, M.A. Caminero, E. García-Plaza, P.J. Núñez, Additive manufacturing of PLA structures using fused deposition modelling: Effect of process parameters on mechanical properties and their optimal selection, Materials and Design 124 (2017) 143-157.

21. N. Zohdi, R.C. Yang, Material Anisotropy in Additively Manufactured Polymers and Composites: A Review, Polymers 13 (2021) 3368.
22. M. Popović, M. Pjević, A. Milovanović, G. Mladenović, M. Milošević, Printing parameter optimization of PLA material concerning geometrical accuracy and tensile properties relative to FDM process productivity, Journal of Mechanical Science and Technology, 37 (2023) 697-706.
23. M. Higaeg, I. Balać, A. Grbović, M. Milovančević, M. Jelic, Numerical Modeling of the Porosity Influence on Strength of Structural Materials, Science of Sintering, 51 (2019) 459-467.
24. E. Abdulrazag, I. Balać, K. Čolić, A. Grbović, M. Milovančević, M. Jelic, Numerical Modeling of the Porosity Influence on the Elastic Properties of Sintered Materials, Science of Sintering, 51 (2019) 153-161.
25. S.M.F. Kabir, K. Mathur, A.F.M. Seyam, A critical review on 3D printed continuous fiber - reinforced composites: History, mechanism, materials and properties, Composite Structures 232 (2020) 111476.
26. N. van de Werken, H. Tekinalp, P. Khanbolouki, S. Ozcan, A. Williams, M. Tehrani, Additively manufactured carbon fiber -reinforced composites: State of the art and perspective, Additive Manufacturing 31 (2020) 100962.
27. M. Domingo-Espin, S. Borros, N. Agullo, A.A. Garcia-Granada, G. Reyes, Influence of building parameters on the dynamic mechanical properties of polycarbonate fused deposition modeling parts, 3D Printing and Additive Manufacturing, 1 (2014) 70-77.
28. D. Croccolo, M. De Agostinis, G. Olmi, Experimental characterization and analytical modelling of the mechanical behaviour of fused deposition processed parts made of ABS-M30, Computational Materials Science 79 (2013) 506-518.

Сажетак: *Експериментално су одређене затезне карактеристике узорака типа танких плоча направљених од PET-G материјала ојачаног кратким угљеничним влакнима, а за различите углове депоновања материјала. У адитивној производњи, угао депоновања материјала представља један од кључних параметара процеса штампе који значајно утиче на чврстоћу и крутост готовог производа. За узорке одштампане са углом депоновања 0° добијена је релативно висока просечна вредност затезне чврстоће од 52.2 MPa, у поређењу са вредношћу од 25.4 MPa добијеном за узорке одштампане са углом депоновања 90°. Слично, за узорке одштампане са углом депоновања 0° добијена је значајно виша просечна вредност модула еластичности од 4752 MPa, у поређењу са вредношћу од 1569 MPa добијеном за узорке одштампане са углом депоновања 90°. Анализа преломних површина узорака је извршена применом скенирајуће електронске микроскопије (СЕМ). Анализом слика добијених путем СЕМ-а утврђен је висок запремински удео порозитета. Порозитет, заједно са слабом везом оствареном између два суседна депонована слоја, представља један од кључних фактора за доста ниске вредности затезних карактеристика добијених за узорке одштампане слојевима депонованим управно на правац затезања (угао депоновања 90°).*

Кључне речи*: адитивна производња, угао депоновања материјала, чврстоћа, крутост, угљенична влакна.*